Journal Pre-proof

On-chip single-photon chirality encircling exceptional points

Zhen-Nan Tian , Feng Yu , Xu-Lin Zhang , Kai Ming Lau , Li-Cheng Wang , Jensen Li , C.T. Chan , Qi-Dai Chen

PII: S2709-4723(23)00029-1
DOI: https://doi.org/10.1016/j.chip.2023.100066
Reference: CHIP 100066

To appear in: *Chip*

Received date: 12 July 2023
Revised date: 20 August 2023
Accepted date: 24 August 2023

Please cite this article as: Zhen-Nan Tian , Feng Yu , Xu-Lin Zhang , Kai Ming Lau , Li-Cheng Wang , Jensen Li , C.T. Chan , Qi-Dai Chen , On-chip single-photon chirality encircling exceptional points, *Chip* (2023), doi: https://doi.org/10.1016/j.chip.2023.100066

On-chip single-photon chirality encircling exceptional points

Zhen-Nan Tian[1†], Feng Yu[1†], Xu-Lin Zhang[1*], Kai Ming Lau[2], Li-Cheng Wang[1], Jensen Li[2], C. T. Chan[2,*] & Qi-Dai Chen[1,*]

[1]*State Key Laboratory of Integrated Optoelectronics, College of Electronic Science and Engineering, Jilin University, Changchun 130012, China*
[2]*Department of Physics, The Hong Kong University of Science and Technology, Clear Water Bay, Hong Kong, China*

[†]These authors contributed equally to this work.

*Correspondence: X.L.Z. (xulin_zhang@jlu.edu.cn), C.T.C. (phchan@ust.hk), Q.-D.C. (email: chenqd@jlu.edu.cn).

Exceptional points (EPs), typically defined as the degeneracy points of a non-Hermitian Hamiltonian, have been investigated in various physical systems such as photonic systems. In particular, the intriguing topological structures around EPs have given rise to novel strategies for manipulating photons and the underlying mechanism is especially useful for on-chip photonic applications. Although some on-chip experiments using lasers have been reported, EP-based photonic chips working in the quantum regime have been largely elusive. Here, we propose a single-photon experiment to dynamically encircle an EP in on-chip photonic waveguides possessing passive anti-parity-time symmetry. Photon coincidences measurement reveals a chiral feature of transporting single photons, which can act as a building block for on-chip quantum devices that require asymmetric transmissions. Our findings pave the way for on-chip experimental study on the physics of EPs as well as inspiring applications for on-chip non-Hermitian quantum devices.

INTRODUCTION

Exceptional points (EPs), first introduced in quantum mechanics by investigating parity-time (PT) symmetric systems, are defined as the coalescence of both the eigenvalues and eigenvectors of a non-Hermitian Hamiltonian[1-4]. Recent studies have revealed their intriguing physics in different physical systems which have enabled various applications[5-16]. In particular, the complex eigenvalues around an EP form self-intersecting energy surfaces, a hallmark feature of non-Hermitian systems that allows the exchange of eigenstates via a stroboscopic encircling of the EP in a parameter space[17,18]. Interestingly, if the system evolves dynamically around a closed loop encircling the EP, i.e., changing an eigenstate

in the real-space structure to mimic the looping of the EP in the parameter space, the dynamics is revealed to be chiral[19-30]. This chiral approach for manipulating waves without introducing chiral structures is unique to non-Hermitian systems, as its realization requires the breakdown of adiabaticity which is a result of non-Hermiticity[31-33].

Most of the studies on the dynamical encirclement of EPs rely on the platform of photonic waveguides[20-30], since it is quite convenient to design a variation of the structure along the waveguiding direction in order to mimic the EP encirclement process. Meanwhile, photonic waveguides are basic elements on a photonic chip. Therefore, the dynamical EP encirclement process would be quite useful for manipulating photons on photonic chips. Although a few EP-related photonic chips have been reported[22-30], the experiments were conducted in the classical regime with lasers being the source. Photonic chips are also powerful platform for exploring quantum phenomenon and associated applications where single photons or multi-photons are used as the information processing carrier. However, the corresponding non-Hermitian experiments remain largely absent.

In this work, we propose an experiment that realizes the dynamical encircling of an EP on a photonic chip towards single-photon manipulations and applications. We design a passive anti-parity-time (anti-PT) symmetric photonic system which supports a second-order EP. The unique topological structure of anti-PT symmetric non-Hermitian systems allows the fact that the eigenmodes that can be used for chiral mode switching lie in the PT-broken phase. As a result, single-photon states employing path-encoding or polarization-encoding can be conveniently used for on-chip asymmetric transmission applications. We perform experiments using both lasers and single-photons through coincidences measurement to verify the EP-encirclement induced chiral photon transmission phenomenon. The proposed system has the potential to become a building block of on-chip asymmetric quantum devices.

RESULTS AND DISCUSSION

EP encircling in on-chip passive anti-PT-symmetric systems. Fig. 1a depicts a schematic diagram of our experimental system which consists of three elliptical waveguides with the center one being lossy. Similar non-Hermitian architectures have been studied before based on microwave platforms[16] and integrated photonic platforms[29,30] using classical light. In this work, we employed femtosecond laser direct writing techniques[34-36] to fabricate the device in boroaluminosilicate glasses and will show measurement results using both classical light and single photons. Our technique allows the fabrication of three-dimensional waveguide arrays and the proposed idea may inspire the design of three-dimensional on-chip non-Hermitian devices. In our system, the straight waveguide S exhibits a loss of ~40 dB/cm, which is achieved by re-exposing the waveguide at equally-spaced points (see Methods).

This technique can create an array of scatterers that induces significant scattering/transmission losses for photons propagating in waveguide S. The loss of a single scatterer is highly tunable since it strongly depends on the exposure time and laser power (Fig. 1c). In the defined "EP encircling region" (with length L = 14 mm), the two gap distances g_1 and g_2 are designed to be varying (also see Fig. 1b for top view) such that an EP is dynamically encircled. We refer to the two end facets of waveguide 1 as port 1 and 1' and so forth for waveguide 2.

Electromagnetic waves propagating in the paraxial waveguides system is governed by a Schrodinger-like equation $i\partial_z|\psi(z)\rangle + H(z)|\psi(z)\rangle = 0$, and the 3×3 non-Hermitian Hamiltonian reads:

$$H(z) = \begin{pmatrix} 0 & \kappa_1(z) & 0 \\ \kappa_1(z) & i\gamma & \kappa_2(z) \\ 0 & \kappa_2(z) & \delta \end{pmatrix}, \quad (1)$$

where κ_1 and κ_2 are coupling coefficients that can be determined from g_1 and g_2 (inset of Fig. 2a), $\gamma = 6\times10^{-5}k_0$ denotes the loss of waveguide S with k_0 being the vacuum wave number, and δ is a detuning parameter (see Supplementary materials, Sec. I for details on fitting the Hamiltonian). The eigenvalues of the Hamiltonian are the change of the waveguide propagation constant introduced to that of an individual lossless waveguide. We label eigenmodes polarized along the y-axis as vertical-polarized modes (V-modes) and study their EPs at wavelength of 810 nm in a g–α–δ 3D parameter space, where we have introduced $g = (g_1+g_2)/2$ and $\alpha = (g_1-g_2)/(g_1+g_2)$. Fig. 2a plots the positions of all the EPs (of second-order) which form two types of exceptional lines (ELs). The dashed EL is located on the $\delta = 0$ plane and satisfies $\kappa_1^2 + \kappa_2^2 = \gamma^2/4$. The solid ELs located at $\kappa_1 = \kappa_2 = \sqrt{|\delta|\gamma/2}$ appear in the region $\delta \neq 0$ and their existence is a consequence of the passive anti-PT symmetry of the system. We leave detailed derivations and discussions on the origin of the ELs as well as the effective Hamiltonian of the system which is passive anti-PT-symmetric (i.e., anti-PT-symmetric but the diagonal term is shifted by a constant) to Supplementary materials, Sec. II, and here we only focus on the EP (see the yellow star) in a g–α 2D parameter space with a fixed value $\delta = 9\times10^{-6}k_0$ (see the grey surface).

Fig. 2b and c plot respectively the real part and imaginary part of the eigenvalues E_H of the Hamiltonian in the g–α parameter space. An EP (marked by the star) can be found as the coalescence of the red sheet and the blue sheet. This EP links the symmetric phase and broken phase (marked by white dashed lines), which can be defined by the symmetry of the eigenfunctions. The inset of Fig. 2c shows the eigenfunctions at g = 10 μm and α = 0 (calculated using COMSOL[37], also see Fig. S1). The

broken eigenmode symmetry confirms that this point is in the broken phase. Considering that the real/imaginary parts of the eigenvalues bifurcate/coalesce there, we can safely state that our system is passive anti-PT-symmetric.

Now we create a loop to encircle the EP, with the above point in the broken phase as the starting/end point (see the loop in Fig. 2a). The loop formula is given in Methods, following which the sample in Fig. 1a was fabricated. A wave incident through port 1 or 2 and exit through port 1' or 2' follows a counter-clockwise loop, while the wave excited through port 1' or 2' leads to a clockwise-loop process. We solve the Hamiltonian equation (see Fig. S2 for details) with these four ports being excited respectively, and summarize the state evolution trajectories on the energy sheets in Fig. 2d-g. We should emphasize that the process in Fig. 2f is more complicated than the other three, since the initial state will encounter a nearly degenerate region (which is marked by the yellow dashed line in Fig. 2b) which is resulted from the exceptional line on the $\delta = 0$ plane in Fig. 2a. When crossing this region, the power is almost equally redistributed into two eigenstates so that we have plotted the evolution trajectory on both the red and grey sheets there (also see Fig. S2 for a more detailed explanation). Fortunately, these complicated evolution details will not affect the mode conversion results, since we find that the output state for counter-clockwise loops is always the mode localized in waveguide 2 (Fig. 2d and e), whereas clockwise loops result in a final state in waveguide 1 (Fig. 2f and g). This is the phenomenon of chiral mode switching, which has been realized in passive PT-symmetric systems for symmetric/antisymmetric modes, i.e., coupled modes localized in two waveguides[21,24]. In contrast, our system enables the chiral transmission of on-chip fundamental modes that are bounded in only one waveguide because of the topological structure of passive anti-PT-symmetric energy surfaces. The mechanism underlying the chiral phenomenon is that the eigenstates tend to stay on the lowest-loss energy sheet (i.e., the blue sheet), otherwise non-adiabatic transitions[19-21] (NATs) from higher-loss sheet to lower-loss sheet would occur (see the NAT in Fig. 2e and f).

Experimental results in the classical regime. We show experimental results using classical laser light at 810 nm (MDL-III, CNI). Fig. 3a-d show the output images (measured by XG500, XWJG) of the V-modes with excitations at different ports. When port 1 or port 2 is excited which corresponds to a counter-clockwise loop to encircle the EP, the output power in waveguide 2 is always significantly larger than that in waveguide 1 (Fig. 3a and b). If we consider waveguide 2 only, the output power in Fig. 3a (~2.78 mW) is much higher than that in Fig. 3b (~0.39 mW). This is due to the fact that the process that is adiabatic (i.e., port 1 in, port 2' out, also see Fig. 2d) would exhibit a lower loss than that with a NAT (i.e., port 2 in, port 2' out, also see Fig. 2e). To further demonstrate this point, we depict in Fig. 3e and f the top-view light diffraction patterns in the device for the above two cases

(photographed by Zyla 5.5 sCMOS, Andor). Since light in waveguide S can be strongly diffracted by the array of scatterers and then captured by our camera, we have lowered these "noises" when plotting Fig. 3e and f in order to make the patterns in waveguide 1 and 2 more clear. Fig. 3e shows an adiabatic transfer of light from waveguide 1 to waveguide 2, whereas Fig. 3f depicts a process with a NAT and light also exits the device via port 2' but with a much lower intensity. The clockwise route can be investigated using the same way, as shown in Fig. 3c and d where the output mode is mainly localized in waveguide 1. These measurements clearly demonstrate the chiral mode switching dynamics, and the NAT as indicated by the power difference is another evidence of such dynamics.

The bandwidth of the chiral phenomenon was studied using a tunable laser (range 730 to 860 nm, Tsunami, Spectra-Physics). We measured the S parameters $S_{m,n}$ of the system, which is defined as the transmission from port n to port m, where m, n = 1, 2, 1', or 2'. Fig. 3g and h plot the ratio of S parameters (see the inset for definitions) for counter-clockwise loops and clockwise loops, respectively. We find that in the grey region (~790 to 820 nm), $S_{2',1}$ and $S_{2',2}$ are the predominant S parameters for counter-clockwise loops, while $S_{1,1'}$ and $S_{1,2'}$ dominate the output for clockwise loops. These results indicate the EP-encirclement induced chiral mode switching. All the above measurements were performed for the V-modes, and we also measured the S parameters for horizontal-polarized modes (H-modes that are polarized along the x-axis). The corresponding results are given in Fig. 3i and j, where the chiral mode switching behavior can also be found but in a different wavelength range (~740 to 780 nm). Such difference should be attributed to dispersion of the eigenmodes as well as the birefringence of the fabricated waveguides. Full results of the S parameters are given in Fig. S4 and S5.

Experimental results in the single-photon regime. We performed experiments in the single-photon regime to show that the above chiral transmission phenomenon also applies to single photons. In the quantum regime, the eigenstates supported in the system are richer than those in the classical system. More specifically, at the starting/end point of the encircling loop, the waveguides system supports classical-like states including $|1_1 0_S 0_2\rangle$, $|0_1 1_S 0_2\rangle$ and $|0_1 1_S 0_2\rangle$, where the subscript and the number indicate respectively the waveguide and the photon number within. Moreover, the quantum system also supports superposition states that have no classical counterparts such as $\left(|1_1 0_S 0_2\rangle + e^{i\varphi}|0_1 0_S 1_2\rangle\right)/\sqrt{2}$ where φ depicts a phase. These quantum states are often used on photonic chips for various applications. Therefore, we need to verify whether these single-photon states can be employed for the chiral transmission by dynamically encircling the EP.

The experimental setup is depicted in Fig. 4a, where pairs of indistinguishable photons at 810 nm

were generated by a BBO crystal. One photon was launched into one port of the fabricated sample and the other photon was propagating in an optical fibre. We used two avalanche photodetectors at the output side of the system to measure their photon coincidences (see Methods), which can demonstrate the evolution dynamics of single photons in the device.

We first test the dynamics of the states $|1_1 0_S 0_2\rangle$ and $|0_1 0_S 1_2\rangle$, and single photons can enter and exit the sample via port 1, 2, 1', or 2'. The measured photon coincidences at different output ports as a function of the input port are summarized in Fig. 4b and c for the V-modes. Fig. 4b shows that for counter-clockwise loops, the photon coincidence measured at port 2' is considerably larger than that at port 1', no matter via which port the single photon was launched. The situation is just opposite for clockwise loops in Fig. 4c, where port 1 always shows the largest photon coincidence. In addition, for either counter-clockwise loops or clockwise loops, the photon coincidence of the adiabatic case (i.e., input from port 1 or port 2') is also higher than that of the case with NATs (i.e., input from port 2 or port 1').

We then test the superposition states by adding a 1:1 directional coupler (with port A and B) before the sample chip, and superposition states $\left(|1_1 0_S 0_2\rangle + e^{i\varphi}|0_1 0_S 1_2\rangle\right)/\sqrt{2}$ can be generated at the input side of the sample. Here φ denotes a phase difference which is equal to $\pi/2$ by choosing a proper length of the directional coupler in our experiment, but its value does not affect the measurement results since the device exhibits a chiral transmission feature. The measured photon coincidences are given in Fig. 4d and e for counter-clockwise loops and clockwise loops, respectively, where the chiral phenomenon is also observed. Therefore, by the dynamical encirclement of a second-order EP in the proposed passive anti-PT-symmetric system, we have realized the on-chip chiral transport of single photons, as single photons will most probably exit the device via waveguide 2 for left-to-right transmissions while via waveguide 1 for right-to-left transmissions. This chiral strategy would be useful for on-chip quantum applications that involve the path-encoding or polarization-encoding of single photons[38,39]. For comparison, we also test the dynamics of the H-modes and show the corresponding results in Fig. 4f-i, where the chiral dynamics does not occur at 810 nm.

Conclusion. To conclude, we have investigated a passive anti-PT-symmetric system in the single-photon regime and revealed the topological structure around a second-order EP of the system. By dynamically encircling the EP in a designed parameter space, we have realized the on-chip chiral transport of single photons, which has the potential to act as the building block of on-chip quantum devices that require an asymmetric transmission feature. The re-exposure technique in our experimental setup allows us to introduce highly tunable loss to the waveguide, making the

experimental platform quite useful for the exploration of non-Hermitian quantum physics. The femtosecond laser direct writing technique can be employed to fabricate three-dimensional on-chip devices[34-36], therefore three-dimensional non-Hermitian single-photon manipulation schemes are expected to be developed in the future. Meanwhile, the functionality of the fabricated devices (e.g., directional coupler) is reconfigurable by using a secondary direct writing technique[40]. A current trend for quantum photonic integrated circuits is to combine multiple materials and platforms in order to fully make use of their respective advantages[41]. In this sense, in addition to its advantage of three-dimensional integration and reconfiguration, the proposed platform is expected to be co-integrated with other quantum-photonic technologies to make up its limitation in terms of integrated quantum sources and detectors. Nitrogen-vacancy color centers in diamonds, which can also be prepared by using femtosecond laser direct writing techniques[42], are good candidates for on-chip single photon sources. Integrating semiconductor single-photon avalanche photodiodes[43] with the proposed photonic chip via heterogeneous approach is a promising solution to the detecting problem. We expect the proposed platform to play a key role in the next generation high-performance wafer-scale quantum photonic integrated circuits.

METHODS

Sample fabrication. The waveguides were fabricated inside boroaluminosilicate glasses (Corning EAGLE 2000, n = 1.504) and the refractive index contrast between the waveguide and the background is ~0.0025. To fabricate the sample, we focused a Ti:sapphire laser (Light Conversion Carbide 5W, repetition rate of 1 MHz, pulse energy of 200 nJ and pulse duration of 290 fs) 170 μm below the glass surface using a ×40 microscope (NA = 0.75). An Aerotech system was used to control the motion of the glass in order to write the waveguides. The waveguide exhibits a size of ~6.85 μm × 5.23 μm under a writing speed of 40 mm/s. The transmission loss in waveguides 1 and 2 is ~0.3dB/cm, which is significantly lower than that in waveguide S.

Re-exposure technique to introduce losses. The loss in waveguide S was introduced using a re-exposure technique. To be specific, we first fabricated a normal waveguide S and then equally-spaced points in waveguide S were re-exposed to introduce scatterers. The exposure time is 10 ms with the laser power of 140 mW and the distance between adjacent points is ~10 μm. Under these conditions, the scattering loss induced by each scatterer was measured to be ~0.04dB, corresponding to a transmission loss in waveguide S of 40 dB/cm.

Quantum measurement. As depicted in Fig. 4a, a continuous-wave pump laser at 405 nm is used as the source. We used a half wave plate (HWP) and a polarization beam splitter (PBS) to manipulate the

polarization and intensity of the beam. After going through a Beta Barium Borate (BBO) crystal, indistinguishable pairs of photons at 810 nm were generated. We then used an HWP and a quarter wave plate (QWP) to control the polarization of each single photon. One single photon was injected into a single-mode fiber (SMF) and finally collected by an avalanche photodetector (APD). The other single photon was injected into the sample (the input port can be port 1, port 2, port 1', or port 2') and another APD was used at the corresponding output port to collect the single photon. Finally, we performed coincidence measurement based on the data collected by the two APDs. In the measurement of Fig. 4d,e,h,i, we have added a directional coupled (DC) before the device in order to generate the superposition states. The DC with a splitting ratio of 1:1 consists of double waveguides on a chip, while our device was fabricated on another chip. We have aligned the two chips but there are still coupling losses. As a result, the measured photon coincidences in Fig. 4d,e,h,i are much lower than those in Fig. 4b,c,f,g.

Formula of the encircling loop. The loop in the g-α parameter space takes the form: $g_1(z)=\cos\left(2\pi z/L+\pi/4\right)\sqrt{32\cos^2\left(2\pi z/L\right)+25\sin^2\left(2\pi z/L\right)}+6$ and $g_2(z)=\sin\left(2\pi z/L+\pi/4\right)\sqrt{32\cos^2\left(2\pi z/L\right)+25\sin^2\left(2\pi z/L\right)}+6$, where the unit is in μm. Then by defining $g=(g_1+g_2)/2$ and $\alpha=(g_1-g_2)/(g_1+g_2)$, we can study the system in the g-α parameter space.

Acknowledgements

This work was supported by National Natural Science Foundation of China (NSFC) under Grants #61825502, #11974140 and #61827826. Work done in Hong Kong was supported by RGC Hong Kong (N_HKUST608/17, AoE/P-502/20 and C6013-18G-A) and by the Croucher Foundation.

REFERENCES

[1] Bender, C. M. & Boettcher, S. Real spectra in non-Hermitian Hamiltonians having PT symmetry. *Phys. Rev. Lett.* **80**, 5243-5246 (1998).
[2] Berry, M. V. Physics of nonhermitian degeneracies. *Czech. J. Phys.* **54**, 1039-1047 (2004).
[3] El-Ganainy, R. *et al*. Non-Hermitian physics and PT symmetry. *Nat. Phys.* **14**, 11-19 (2018).
[4] Li, A. et al. Exceptional points and non-Hermitian photonics at the nanoscale, *Nat. Nanotechnol.* **18**, 706 (2023).
[5] Guo, A. *et al*. Observation of PT-symmetry breaking in complex optical potentials. *Phys. Rev. Lett.* **103**, 093902 (2009).
[6] Rüter, C. E. *et al*. Observation of parity–time symmetry in optics. *Nat. Phys.* **6**, 192-195 (2010).
[7] Ding, K., Ma, G., Xiao, M., Zhang, Z. Q. & Chan, C. T. Emergence, coalescence, and topological properties of multiple exceptional points and their experimental realization. *Phys. Rev. X* **6**, 021007 (2016).

[8] Peng, B. *et al*. Loss-induced suppression and revival of lasing. *Science* **346**, 328-332 (2014).
[9] Hodaei, H., Miri, M., Heinrich, M., Christodoulides, D. N. & Khajavikhan, M. Parity-time-symmetric microring lasers. *Science* **346**, 975-978 (2014).
[10] Chen, W., Özdemir, S. K., Zhao, G., Wiersig, J. & Yang, L. Exceptional points enhance sensing in an optical microcavity. *Nature* **548**, 192-196 (2017).
[11] Hodaei, H. *et al*. Enhanced sensitivity at higher-order exceptional points. *Nature* **548**, 187-191 (2017).
[12] Assawaworrarit, S., Yu, X. & Fan, S. Robust wireless power transfer using a nonlinear parity-time-symmetric circuit. *Nature* **546**, 387-390 (2017).
[13] Zhao, H. *et al*. Non-Hermitian topological light steering. *Science* **365**, 1163-1166 (2019).
[14] Xu, H., Mason, D., Jiang, L. & Harris, J. G. E. Topological energy transfer in an optomechanical system with exceptional points. *Nature* **537**, 80-83 (2016).
[15] Wang, S. *et al*. Arbitrary order exceptional point induced by photonic spin-orbit interaction in coupled resonators. *Nat. Commun.* **10**, 832 (2019).
[16] Zhang, X. L., Jiang, T. & Chan, C. T. Dynamically encircling an exceptional point in anti-parity-time symmetric systems: asymmetric mode switching for symmetry-broken modes. *Light Sci. Appl.* **8**, 88 (2019).
[17] Dembowski, C. *et al.* Experimental observation of the topological structure of exceptional points. *Phys. Rev. Lett.* **86**, 787-790 (2001).
[18] Gao, T. *et al.* Observation of non-Hermitian degeneracies in a chaotic exciton-polariton billiard. *Nature* **526**, 554-558 (2015).
[19] Hassan, A. U., Zhen, B., Soljačić, M., Khajavikhan, M. & Christodoulides, D. N. Dynamically encircling exceptional points: exact evolution and polarization state conversion. *Phys. Rev. Lett.* **118**, 093002 (2017).
[20] Doppler, J. *et al*. Dynamically encircling an exceptional point for asymmetric mode switching. *Nature* **537**, 76-79 (2016).
[21] Zhang, X. L., Wang, S. B., Hou, B. & Chan, C. T. Dynamically encircling exceptional points: in situ control of encircling loops and the role of the starting point. *Phys. Rev. X* **8**, 021066 (2018).
[22] Liu, Q. et al. Efficient mode transfer on a compact silicon chip by encircling moving exceptional points. *Phys. Rev. Lett.* **124**, 153903 (2020).
[23] Li, A. et al. Hamiltonian hopping for efficient chiral mode switching in encircling exceptional points. *Phys. Rev. Lett.* **125**, 187403 (2020).
[24] Yoon, J. W. *et al*. Time-asymmetric loop around an exceptional point over the full optical communications band. *Nature* **562**, 86-90 (2018).
[25] Choi, Y., Hahn, C., Yoon, J. W., Song, S. H. & Berini, P. Extremely broadband, on-chip optical nonreciprocity enabled by mimicking nonlinear anti-adiabatic quantum jumps near exceptional points. *Nat. Commun.* **8**, 14154 (2017).
[26] Yu, F., Zhang, X. L., Tian, Z. N., Chen, Q. D. & Sun, H. B. General rules governing the dynamical encircling of an arbitrary number of exceptional points, *Phys. Rev. Lett.* **127**, 253901 (2021).
[27] Shu, X. et al. Fast encirclement of an exceptional point for highly efficient and compact chiral mode converters, *Nat. Commun.* **13**, 2123 (2022).
[28] Li, A. et al. Riemann-encircling exceptional points for efficient asymmetric polarization-locked devices, *Phys. Rev. Lett.* **129**, 127401 (2022).
[29] Feng, Z. & Sun, X. Harnessing dynamical encircling of an exceptional point in anti-PT-symmetric integrated photonic systems, *Phys. Rev. Lett.* **129**, 273601 (2022).
[30] Wei, Y. et al. Anti-parity-time symmetry enabled on-chip chiral polarizer, *Photonics Res.* **10**, 76 (2022).
[31] Uzdin, R., Mailybaev, A. & Moiseyev, N. On the observability and asymmetry of adiabatic state flips generated by exceptional points. *J. Phys. A Math. Theor.* **44**, 435302 (2011).
[32] Gilary, I., Mailybaev, A. A. & Moiseyev, N. Time-asymmetric quantum-state-exchange

mechanism. *Phys. Rev. A* **88**, 010102 (2013).
[33] Milburn, T. J. *et al*. General description of quasiadiabatic dynamical phenomena near exceptional points. *Phys. Rev. A* **92**, 052124 (2015).
[34] Xu, X. Y., Wang, X. W., Chen, D. Y., Smith, C. M. & Jin, X. M. Quantum transport in fractal networks, *Nat. Photon.* **15**, 703 (2021).
[35] Zhang, X. L. et al. Non-Abelian braiding on photonic chips. *Nat. Photon.* **16**, 390–395 (2022).
[36] Sun, Y. K. et al. Non-Abelian Thouless pumping in photonic waveguides. *Nat. Phys.* **16**, 1080-1085 (2022).
[37] www.comsol.com.
[38] Politi, A., Cryan, M. J., Rarity, J. G., Yu, S. & O'Brien, J. L. Silica-on-silicon waveguide quantum circuits. *Science* **320**, 646-649 (2008).
[39] Llewellyn, D. *et al*. Chip-to-chip quantum teleportation and multi-photon entanglement in silicon. *Nat. Phys.* **16**, 148-153 (2020).
[40] Yu, F. *et al*. Resetting directional couplers for high-fidelity quantum photonic integrated chips. *Opt. Lett.* **46**, 5181-5184 (2022).
[41] Moody, G. *et al*. 2022 Roadmap on integrated quantum photonics. *J. Phys. Photonics* **4**, 012501 (2022).
[42] Gao, S. *et al*. Narrow-linewidth diamond single-photon sources prepared via femtosecond laser. *Appl. Phys. Lett.* **120**, 023104 (2022).
[43] Zhang, B. *et al*. High performance InGaAs/InP single-photon avalanche diode using DBR-metal reflector and backside micro-lens. *J. Lightw. Technol.* **40**, 3832-3838 (2022).

Figures and captions

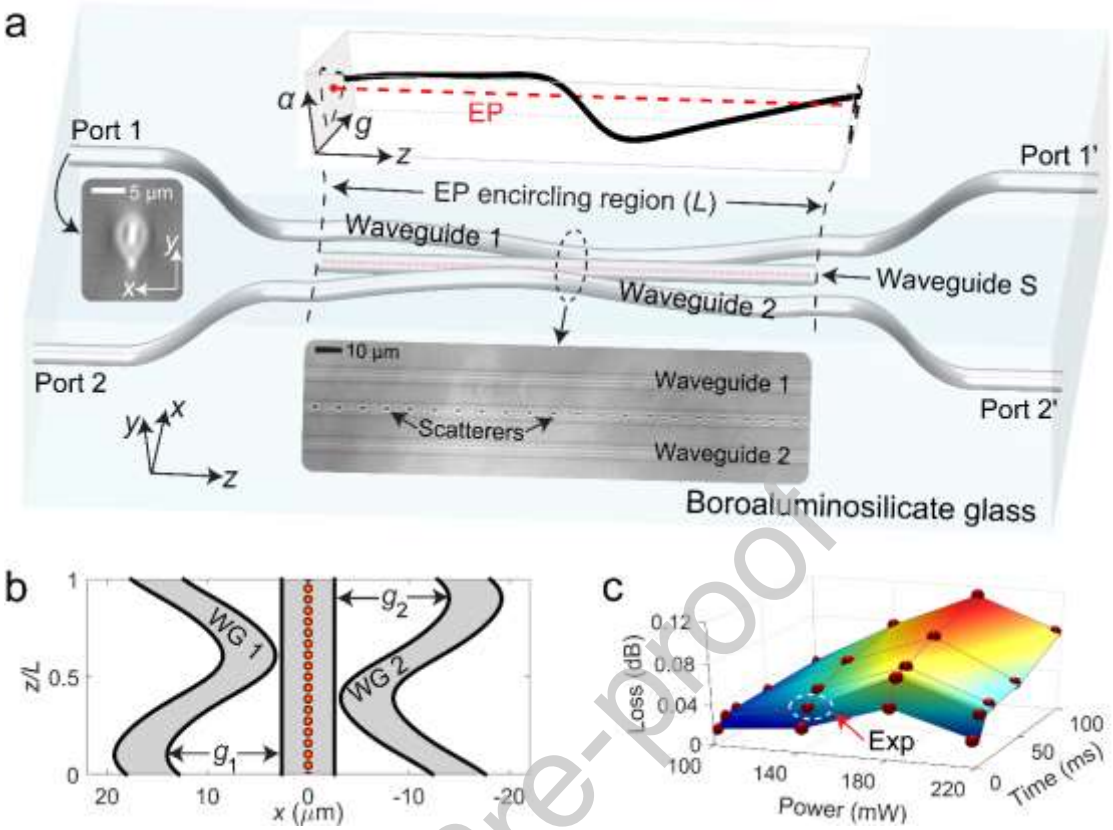

Fig. 1 | a, Schematic diagram of a passive anti-PT-symmetric system consisting of three waveguides in boroaluminosilicate glass. The upper inset depicts that in the EP encircling region, electromagnetic waves or single photons propagating in the system is equivalent to a process that an EP is dynamically encircled in the g-α parameter space. Photographs of the fabricated sample are also given in the inset; **b,** Top-view of the three waveguides in the EP encircling region; **c,** Measured scattering loss of a single scatterer as a function of the exposure time and laser power, where the dashed circle marks the experimental configuration.

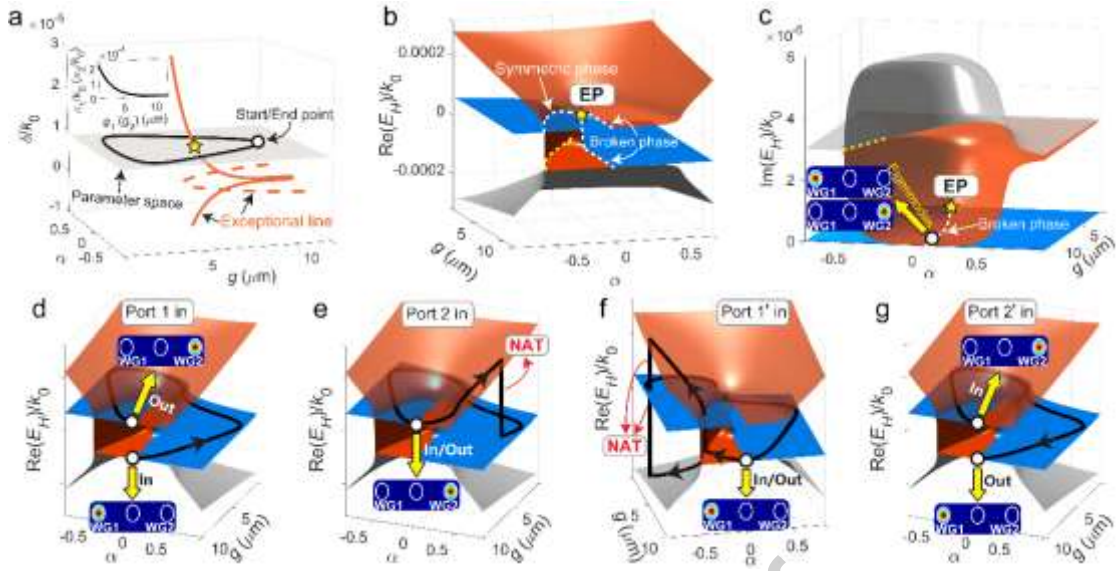

Fig. 2 | a, Calculated positions of EPs which form three ELs (orange solid and dashed lines) in the g–α–δ 3D parameter space. The grey plane depicts the g-α 2D parameter space used in experiment where a closed loop (black line) is generated to encircle the EP (yellow star). The inset plots the fitting value of κ_1 (κ_2) as a function of g_1 (g_2); **b,c,** Real part **(b)** and Imaginary part **(c)** of the eigenvalues of the non-Hermitian Hamiltonian in the g-α parameter space. The symmetric phase and broken phase are marked by the white dashed lines. The starting/end point of the loop lying on the broken phase is marked by the circle with the corresponding eigenfield distributions given in the inset; **d-g,** Trajectories of the state evolution on the real part of the energy surface with port 1 **(d)**, port 2 **(e)**, port 1' **(f)**, and port 2' **(g)** as the excitation port. All the simulations were performed for the V-modes at 810 nm.

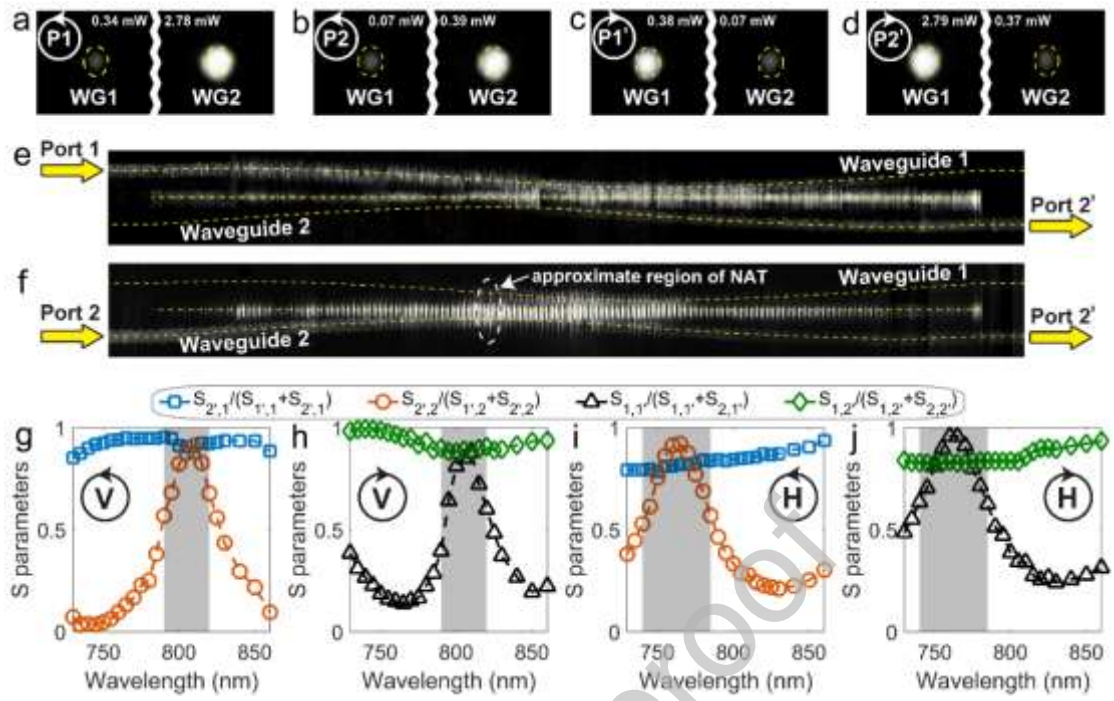

Fig. 3 | a-d, Measured diffraction patterns of laser (~810 nm) at the output facet with port 1 **(a)**, port 2 **(b)**, port 1' **(c)**, and port 2' **(d)** being excited. The values of the output power in waveguide 1 and waveguide 2 are indicated in the inset; **e,f,** Top-view light diffraction patterns in the device with port 1 **(e)** and port 2 **(f)** being the input port. The yellow dashed lines mark the center line of each waveguide. The working mode is the V-mode in **a-f**; **g,h,** Ratios of the measured S parameters as a function wavelengths for the V-modes, where the chiral mode switching phenomenon can be observed in the grey region; **i,j,** Items shown are the same as those in **g,h** except for the H-modes.

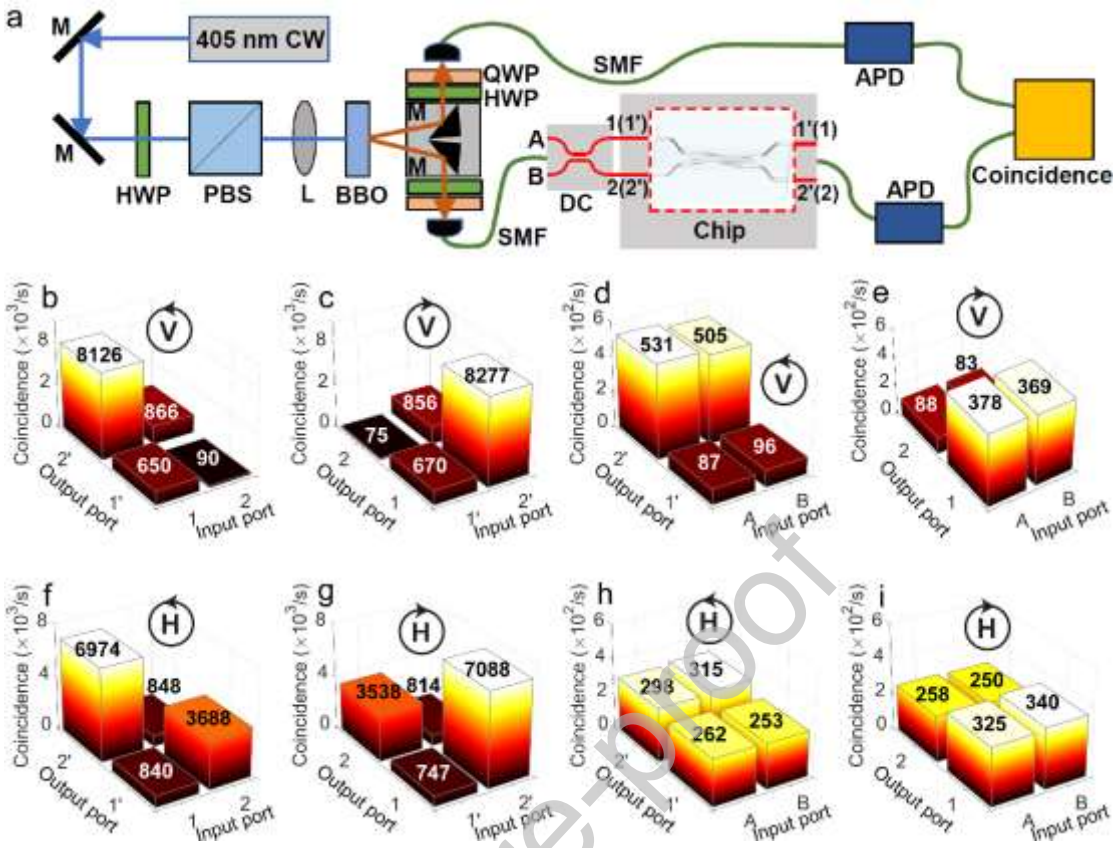

Fig. 4 | a, Experimental setup of the quantum measurement (see Methods for details); **b-e,** Measured photon coincidences per second for the V-modes when single-waveguide state (e.g., $|1_1 0_S 0_2\rangle$ or $|0_1 0_S 1_2\rangle$) **(b,c)** and their superposition states **(d,e)** are excited, where the phenomenon of chiral transport of single photons occurs. The encircling direction is indicated in the inset; **f-i,** Items shown are the same as those in **b-e** except for the H-modes, where the chiral phenomenon is absent at 810 nm. The directional coupler (shorted for DC in **a**) is removed in the measurement of **b**, **c, f** and **g**.

Declaration of interests

☒ The authors declare that they have no known competing financial interests or personal relationships that could have appeared to influence the work reported in this paper.

☐The authors declare the following financial interests/personal relationships which may be considered as potential competing interests: